HHS Public Access

Author manuscript

J Pharm Sci. Author manuscript; available in PMC 2017 May 01.

Published in final edited form as:

J Pharm Sci. 2016 May ; 105(5): 1603–1613. doi:10.1016/j.xphs.2016.02.009.

Novel Ricin Subunit Antigens with Enhanced Capacity to Elicit Toxin-Neutralizing Antibody Responses in Mice

Newton Wahome[1,#], **Erin Sully**[2,#], **Christopher Singer**[4,#], **Justin C. Thomas**[1,a], **Lei Hu**[1,b], **Sangeeta B. Joshi**[1], **David B. Volkin**[1], **Jianwen Fang**[5,c], **John Karanicolas**[6], **Donald J. Jacobs**[4], **Nicholas J. Mantis**[2,3], and **C. Russell Middaugh**[1,*]

[1]Macromolecule and Vaccine Stabilization Center, Department of Pharmaceutical Chemistry, University of Kansas, Lawrence, KS 66047

[2]Division of Infectious Disease, Wadsworth Center, New York State Department of Health, Albany, NY 12208

[3]Department of Biomedical Sciences, University at Albany School of Public Health, Albany, NY 12201

[4]Department of Physics and Optical Science, University of North Carolina at Charlotte, Charlotte, NC 28223

[5]Applied Bioinformatics Laboratory, University of Kansas, Lawrence, KS 66047

[6]Center for Computational Biology and Department of Molecular Biosciences, University of Kansas, Lawrence, KS 66045

Abstract

RiVax is a candidate ricin toxin subunit vaccine antigen that has proven to be safe in human Phase I clinical trials. In this study we introduced double and triple cavity-filling point mutations into the RiVax antigen with the expectation that stability enhancing modifications would have a beneficial

[*]To whom correspondence should be addressed: C. Russell Middaugh, Macromolecule and Vaccine Stabilization Center, Department of Pharmaceutical Chemistry, 2030 Becker Drive, Lawrence, KS 66047. telephone: (785) 864-5813; fax: (785) 864-5736; middaugh@ku.edu.

[#]Authors of equal contribution

[a]Present address: Eli Lilly & Company, Indianapolis, IN, 46285

[b]Present address: Pfizer, Pearl River, NY 10965

[c]Present address: National Cancer Institute, Bethesda, MD 20892

Donald J. Jacobs, Department of Physics and Optical Science, University of North Carolina at Charlotte, Charlotte, NC 28223. telephone: (704) 687-8143; fax: (704) 687-3160, djacobs1@uncc.edu

Nicholas J. Mantis, Division of Infectious Disease, Wadsworth Center, 120 New Scotland Avenue, Albany, NY 12208. telephone: (518) 473-7487; fax: (518) 402 4773; nicholas.mantis@health.ny.gov

Author Contributions Statement

NW, JCT, SBJ, DBV, and CRM wrote the biophysical portion of the manuscript, ES and NJM wrote the immunology section, and CS and DJJ performed the computational analysis. NW, JCT and LH conducted the biophysical experiments, ES performed the mouse experiments, and CS analyzed the mutants with the mDCM computational model. The single point mutation precursors were computed by JCT, JF and JK. All authors reviewed the manuscript.

Conflict of Interest Disclosure

JCT, JK, NW, and CRM are co-inventors on a provisional patent application regarding the RiVax mutants described in the paper

effect on overall immunogenicity of the recombinant proteins. We demonstrate that two RiVax triple mutant derivatives, RB (V81L/C171L/V204I) and RC (V81I/C171L/V204I), when adsorbed to aluminum salts adjuvant and tested in a mouse prime-boost-boost regimen were 5 to 10-fold more effective than RiVax at eliciting toxin-neutralizing serum IgG antibody (TNA) titers. Increased TNA values and seroconversion rates were evident at different antigen dosages and within seven days following the first booster. Quantitative stability/flexibility relationships (QSFR) analysis revealed that the RB and RC mutations affect rigidification of regions spanning residues 98 to 103, which constitutes a known immunodominant neutralizing B cell epitope. A more detailed understanding of the immunogenic nature of RB and RC may provide insight into the fundamental relationship between local protein stability and antibody reactivity.

Keywords

Ricin; Computational Biology; Immunology; Vaccines; Protein Structure; Physical stability

Introduction

The advent of structural vaccinology coupled with the capacity to synthesize large amounts of recombinant protein antigens in *Escherichia coli* and other organisms has made subunit vaccines increasingly attractive in the ongoing war against emerging infectious diseases and biothreat agents, including toxins such as ricin for which effective vaccines have proven elusive [1–3]. Ricin is a type II ribosome-inactivating protein (RIPs) derived from the seeds of the castor bean plant (*Ricinus communis*) [4]. In its mature form, ricin is a 64 kDa globular glycoprotein composed of a 34 kDa enzymatic subunit (RTA) joined by a single disulfide bond to a 32 kDa binding subunit (RTB) [5,6]. RTB, a galactose- and N-acetylgalactosamine (Gal/GalNac) lectin, promotes the attachment and entry of ricin into mammalian cells [7,8]. Following endocytosis, RTB mediates the retrograde trafficking of ricin from the plasma membrane to the trans Golgi network (TGN) and the endoplasmic reticulum (ER). Once in the ER, RTA is liberated from RTB and is dislocated across the ER membrane into the cytoplasm [9]. RTA is an RNA *N*-glycosidase that selectively depurates a highly conserved adenosine residue within the sarcin-ricin loop (SRL) of eukaryotic 28s ribosomal RNA [10]. Hydrolysis of the SRL by RTA results in the cessation of cellular protein synthesis, activation of the ribotoxic stress response (RSR), and cell death via apoptosis [11].

Ricin is a potential biothreat agent and remains a concern for military and public health officials in the United States, as evidenced by ricin being classified by the Centers for Disease Control and Prevention's (CDC) within the Select Agents and Toxins [3,12]. Efforts to develop a ricin toxin vaccine for use by military personnel and certain civilian populations (*e.g.*, emergency first responders and laboratory staff) initially focused on a formalin-inactivated toxoid. Although the toxoid vaccine proved to be highly efficacious in rodents and non-human primate its development for use in humans was abandoned because of manufacturing and safety concerns [13,14].

For more than a decade, efforts have been aimed at the development of a recombinant subunit vaccine, with particular emphasis on attenuated derivatives of the toxin's 267 amino

acid enzymatic subunit, RTA [15,16]. One of the most advanced candidate subunit antigens is RiVax™, an *Escherichia coli*-based recombinant form of RTA that contains two point mutations: V76M and Y80A [17,18]. The Y80A mutation attenuates RTA's RNA *N*-glycosidase activity, while the V76M mutation eliminates RTA's capacity to elicit vascular leak syndrome (VLS) [17,18]. X-ray crystallography indicates that the V76M and Y80A substitutions do not alter the tertiary structure of RTA [19]. In mice, RiVax immunization by the intramuscular (i.m.), subcutaneous (s.c.) or intradermal (i.d.) routes elicits toxin-specific serum IgG Abs that are sufficient to confer protection against a lethal dose of ricin administered by systemic (intraperitoneal) or mucosal (aerosol) routes [16,17,20–23]. Moreover, Phase I clinical trials have demonstrated that RiVax is safe in healthy human volunteers [24,25].

The Phase Ib clinical trials did, however, reveal a notable shortcoming associated with RiVax; even after three intramuscular immunizations with 100 μg RiVax adsorbed to Alhydrogel, toxin-neutralizing serum antibody titers remained relatively modest [24,25]. This finding was not unexpected, considering that inert, non-self-assembled subunit vaccines are notorious for being poorly immunogenic. Nonetheless, RiVax may be unusual in this respect as evidenced by studies in our laboratory that compared the onset of toxin-neutralizing antibodies in mice following two parenteral immunizations with RiVax or a recombinant protective antigen (rPA) from anthrax, each adsorbed to Alhydrogel. Whereas anthrax toxin neutralizing antibodies were achieved within days following the booster immunization, ricin-specific neutralizing antibodies were not detectable for weeks [26].

One obvious strategy to augment the overall immunogenicity of RiVax is through the use of next generation adjuvants [1]. We recently reported that a novel Type II heat labile enterotoxin (HLTs) when co-administered with RiVax (without Alhydrogel) enhanced the onset of toxin-neutralizing antibodies and protective immunity [20]. However, adjuvants themselves may not be sufficient to achieve maximal immunogenicity of RiVax. There is evidence to suggest that the failure of RTA-based antigens in general to elicit high titer toxin-neutralizing antibodies may be due to factors intrinsic to RTA, such as its propensity to partially unfold in the absence of its partner, RTB [27]. If that is the case, enhancing the immunogenicity of RiVax may require a structure-based redesign of the antigen itself. Reengineering RTA is not a new concept, as the US Army has produced truncated (e.g., removing residues 199–267) and disulfide bond stabilized derivatives of RTA that have proven effective at eliciting protective immunity to ricin in mouse models [15,28–30].

With the goal of preserving the RTA's native structure as much as possible, we have chosen a site-directed approach to the redesign of RiVax. In a recent study we used orthogonal and complementary computational protein design approaches to generate a total of 11 single-point mutations in RiVax that were characterized using an array of biophysical and biochemical techniques to assess secondary and tertiary structures, as well as thermostability [31]. One approach applied the Rosetta protein modeling suite [32,33] to the RiVax crystal structure (PDB ID: 3BJG) to generate an ensemble of fifty near-native conformations [34,35]. Each conformation was analyzed to identify under packed regions in the protein core, and then subjected to RosettaDesign to identify small-to-large or isosteric mutations at these sites that were predicted to stabilize the protein by improving packing [36].

This strategy identified several mutations, including V81I, C171L, and V204I. A second design approach utilized a multi-layered filtering scheme to identify mutations predicted to have enhanced stability [37,38]. Predicted stabilizing mutations were created and visually inspected in the Molecular Operating Environment (MOE software suite, V. 2009.10, Chemical Computing Group), which lead to the identification of mutations V18P, C171V and S228K. These single point mutations were introduced onto the RiVax template and subsequently evaluated in a mouse model for the ability to elicit ricin-specific neutralizing antibodies and protective immunity [31]. In this current study, we have now created additional derivatives of the RiVax antigen in which we have combined single-point mutations to generate double and even triple mutants. The resulting combinations of cavity-filling mutations were tested in a mouse model and led to the identification of two derivatives of RiVax, referred to as RiVax-RB and RiVax-RC that are several times more efficient than RiVax at eliciting toxin-neutralizing antibodies.

Methods

Protein production

Plasmids with a tobacco etch virus (TEV)-cleavable, N-terminal hexa-histidine tag containing the RiVax mutants of interest were produced from the parental RiVax plasmid using QuikChange site-directed mutagenesis kit (Life Technologies, San Diego, CA), as described [31]. Introduced mutations were confirmed by sequence analysis of plasmid DNA (Iowa State University Sequencing Facility, Ames, Iowa). RiVax and RiVax derivatives were expressed in *E. coli* BL21 (DE3) pRARE upon induction by isopropyl β-D-1-thiogalactopyranoside (IPTG). The bacterial cells were lysed by sonication and the soluble protein was purified using Ni+-Sepharose affinity chromatography followed by size exclusion chromatography. The histidine tag was cleaved using TEV protease and then followed by Ni+-Sepharose affinity chromatography to remove residual cleaved his-tagged TEV. The cleaved and purified RiVax mutants were then passed through a polymyxin B agarose column. Finally, the RiVax mutants were dialyzed into 20 mM histidine, 300 mM NaCl, diluted 1:1 with a 20% sucrose solution, and stored at −80 °C until further use. Once thawed, the proteins were stored at 4 °C. SDS-PAGE indicated all proteins migrated predominantly as a single monomeric species (> 95%) at the appropriate molecular weight (data not shown).

Assessment of protein stability

Proteins were dialyzed overnight at 4°C into a 20 mM citrate phosphate buffer (pH 7.0) adjusted to an ionic strength of 0.15 by the addition of sodium chloride. The proteins were assayed at a concentration of 0.1 mg/ml for the spectroscopic experiments and 0.5 mg/ml for the DSC studies. For the spectroscopic techniques, spectra were recorded every 2.5 °C from 10 – 75 °C using an equilibration time of 3 min at each temperature. Apparent transition melting temperatures were calculated for each replicate before calculating the average and standard deviation.

Circular dichroism (CD)

Secondary structure stability was assessed by recording CD spectra from 195–260 nm in 1 nm increments with an Applied Photophysics Chirascan-plus CD spectrometer equipped with a four-position, Peltier-controlled cell holder. Measurements were made in a 1 mm pathlength cuvette. Molar ellipticity at 208 nm was plotted as a function of temperature.

Tryptophan fluorescence

Tertiary structure stability was assessed by monitoring tryptophan fluorescence emission from 310–400 nm in 1 nm increments with a Photon Technology International spectrofluorometer equipped with a four-position, Peltier-controlled cell holder. An excitation wavelength of 295 nm was used to selectively excite the lone tryptophan residue. In addition, the aggregation behavior of the proteins was monitored by simultaneously collecting light scattering at the incident wavelength. Light scattering detection was accomplished with a second detector positioned 180° to the detector used to collect tryptophan fluorescence. Tryptophan peak position was determined using a center of spectral mass method[39] and plotted as a function of temperature. This method artificially red-shifted the true peak position by ~ 15 nm but provides better signal/noise ratios and improved precision. For each sample, the light scattering signal at 295 nm was normalized between 0 and 1 and plotted as a function of temperature.

Differential scanning calorimetry

DSC was performed with a MicroCal VP-Capillary DSC. The temperature was ramped from 15 – 75 °C using a ramp rate of 60 °C/h. The sample cell was equilibrated for 15 min at the start temperature before beginning data acquisition. Apparent transition melting temperatures and apparent changes in enthalpy were calculated for each replicate using a non-two-state equilibrium model in Origin 7.0 (OriginLab; Northampton, MA) before calculating the average and standard deviations. Note that we use the word stability in an empirical (not equilibrium) sense.

Mouse handling (ethics statement), immunization studies and serum antibody analysis

BALB/c mice (female, 5–6 weeks of age) were purchased from Taconic Labs (Hudson, NY) and housed at the Wadsworth Center under conventional, specific pathogen-free (SPF) conditions. Experiments involving mice were approved by the Wadsworth Center's Institutional Animal Care and Use Committee (IACUC) under protocol 14–384. The Wadsworth Center complies with the Public Health Service Policy on Humane Care and Use of Laboratory Animals and was issued assurance number A3183-01. The Wadsworth Center is fully accredited by the Association for Assessment and Accreditation of Laboratory Animal Care (AAALAC). Obtaining this voluntary accreditation status reflects that Wadsworth Center's Animal Care and Use Program meets all of the standards required by law, and goes beyond the standards as it strives to achieve excellence in animal care and use.

For immunizations, RiVax antigens were dialyzed against 10 mM histidine (pH 6) and 144 mM sodium chloride and then adsorbed to Alhydrogel® adjuvant (0.85 mg aluminum; E.M. Sergeant, Clifton, NJ) in a final volume of 1 ml. Adsorption was done 1 h prior to each immunization. Unless noted otherwise, the vaccine preparations were administered to mice

by the subcutaneous (s.c.) route on days 0, 10 and 20. Blood was collected from the lateral tail veins of mice on days 17 and 27. Mice were challenged with ricin (10x LD_{50}; ~2 μg/mouse) on day 30 and monitored daily (for up to seven days) for the onset of hypoglycemia, an established measure of morbidity associated with ricin intoxication. Blood glucose levels were determined using an ACCU-CHEK® Aviva System Blood Glucose Meter (Roche Diagnostics). Mice were euthanized when blood glucose levels fell below 20 mg/dL. Ricin toxin-specific ELISAs and assessment of toxin-neutralizing antibody titers using the Vero cell cytotoxicity assay were done as described [40].

Minimum distance constraint model (mDCM)

The relationships between flexibility and stability across the RiVax mutations were computationally assessed using the minimum distance constraint model (mDCM) [41–43]. In the mDCM, protein structure is mapped onto a graph where vertices represent atoms and intramolecular interactions are modeled as edges. Each edge serves as a distance constraint and contributes an energy and entropy. Network rigidity is employed to account for non-additivity in entropy as detailed in two recent reviews [44,45]. An ensemble of constraint topologies that perturb away from the native state structure is generated to represent all accessible conformational states of the protein from the native state to the unfolded state by allowing native packing interactions and H-bonds to break and reform as part of equilibrium fluctuations. Three empirical parameters that reflect solvent interactions are adjusted to fit to experimental DSC measurements. Since technical details can be found elsewhere[41–50], only the procedure used to generate the results reported here are described.

As input to the mDCM, each protein mutant structure was modeled based on the known crystal structure of RiVax (PDBID: 3SRP) using MOE. Given an input protein structure at the all-atom level, the mDCM generates an ensemble of constraint topologies characterized by an intensive global flexibility order parameter defined as the number of independent degrees of freedom per residue. After the three empirical parameters are obtained following established protocols [47,50], the free energy landscape is calculated as a function of temperature and global flexibility order parameter [48]. At temperature, T_{peak}, where heat capacity is a maximum, a thermodynamic average for quantitative stability/flexibility relationships (QSFR) is taken in the native and transition state sub-ensembles, and these QSFR characteristics are compared between RiVax and its mutants.

The backbone flexibility is characterized by the flexibility index (FI), which characterizes the excess degrees of freedom in flexible regions and excess constraints in rigid regions based on a graph rigidity algorithm [46]. In a flexible region the flexibility index is defined as the number of independent degrees of freedom within the region divided by its number of rotatable covalent bonds. In a rigid region, the flexibility index is defined as the number of redundant constraints within the region divided by its number of (non-rotatable) covalent bonds. A (positive, negative) sign is used to denote the region as being (flexible, rigid).

A cooperativity correlation plot (CC-plot) is a symmetric square matrix that quantifies how rigidity and flexibility couples pairs of residues. For a given constraint network, the correlation between residues x and y is zero unless x and y belong to the same flexible or rigid region. For example, if x and y belong to the same rigid region with flexibility index

given by FI_{rig}, then CC(x,y) = CC(y,x) = FI_{rig}. If x and y belong to the same flexible region with flexibility index given by FI_{flx}, then CC(x,y) = CC(y,x) = FI_{flx}. The next step is to take a thermodynamic average over an ensemble of constraint networks. In this report, CC-plots are averaged in the native and transition state ensembles, respectively denoted as NSE and TSE.

Difference CC-plots are calculated as a matrix subtraction $\Delta CC^{NSE}=CC_2^{NSE}-CC_1^{NSE}$ to facilitate comparison between two proteins in their respective NSE. Similar difference CC-plots for the transition state $\Delta CC^{TSE}=CC_2^{TSE}-CC_1^{TSE}$ are also made. To aid in quantifying and visualizing statistical significance in differences, values in a CC-plot or difference CC-plot are transformed into a *signal beyond noise ratio* (SBNR) defined as follows. Considering the NSE and TSE separately, the statistics of the absolute deviations across all matrix elements in a difference CC-plot, defined by $D=|CC_m(x, y) - CC_0(x, y)|$ is first calculated. Then the set of $\{D\}$ from all possible x, y pairs and over all 5 different mutations is collected to obtain the standard deviation, σ. If the absolute value of a CC-plot element is below σ, then SBNR = 0. For a value greater than σ, SBNR = (value − σ)/σ. For a value less than −σ, SBNR = (value + σ)/σ. Note that the definition of *signal to noise ratio* (SNR) is value/σ. Therefore, SBNR is similar to SNR in that it is scaled by the s that reflects noise, but approximately 60% of matrix elements are filtered to zero. The SBNR gives the number of standard deviations beyond one standard deviation, meaning a SBNR > 1 is statistically significant, since SBNR=1 corresponds to SNR=2.

Additional information on the biophysical analysis, immunogenicity, and computation modeling of the RiVax mutants can be found in the supplementary materials.

Results

Design and structural characterization of RiVax derivatives

In a recent report we used the Rosetta software suite to introduce cavity filling point mutations into RiVax with the goal of identifying derivatives that were more immunogenic in mice than RiVax itself. That initial screen resulted in the identification of several antigens that when adsorbed to aluminum salts and tested in mice were slightly more immunogenic than RiVax at eliciting ricin toxin-specific antibodies [31]. In an attempt to further enhance and improve the immunogenicity of RiVax, we produced and purified an additional four derivatives of RiVax with double and triple cavity filling point mutations. As shown in Table 1, the four mutants are RA (V81I/V204I), RB (V81L/C171L/V204I), SA (V18P/C171V), and SB (C171V/S228K). The derivatives displayed CD spectra that were nearly identical to RiVax, with RA displaying slight structure perturbation, indicating that the cavity filling point mutations did not alter the overall secondary structure of RiVax (Fig. 1A). The environment surrounding RTA's active site as measured by tryptophan fluorescence was also similar between RiVax and each of the four RiVax mutants (Fig. 1B).

The thermostability of each of the RiVax mutants, RA, RB, SA, and SB, was assessed using CD, tryptophan fluorescence, light scattering, and DSC (Table 2). CD at 208 nm was followed to assess changes in helical content. Some of the mutations impacted the thermal stability of the helical regions of the proteins and the active site environment[51] as detected

by intrinsic tryptophan fluorescence thermal melts. For the CD melts, relative to RiVax, SA and SB gained ~ 2 °C, and RB gained ~ 1 °C in stability (Fig. 1C). For the fluorescence melts, relative to RiVax, SA and SB shifted ~ 2 °C, and RB gained ~ 1 °C in stability (Fig. 1D). All proteins were prone to temperature-dependent aggregation and precipitation, as indicated by increases in light scattering (Fig. 1E).

We used DSC to obtain a more global perspective of stability changes resulting from the cavity-filling mutations (Fig. 1F). The best fit of the DSC data indicated two thermal transitions. DSC analysis suggested that RTA-based proteins undergo two distinct changes in response to increasing temperature, the first of which was undetected by the spectroscopic techniques described in Figures 1A and 1B. The midpoint of this first structural change in RiVax occurred at ~48 °C and was irreversible, as determined by programming the instrument to scan just past the T_m of the first transition, cool, and then rescan just past the first T_m. Deconvolution of the thermograms permitted an estimation of apparent T_m values and apparent enthalpy changes associated with each transition. None of the four derivatives had any significant shifts in thermal stability in either of the two transition regions. It is unclear what effect the aggregation and precipitation events had on the values tabulated in Table 2.

RiVax derivatives enhance the onset of toxin-neutralizing antibodies

To determine if the cavity-filling mutations affected the immunogenicity of RiVax, groups of mice were primed and then boosted twice at 10-day intervals by the s.c. route with each of the four RiVax cavity filling mutants (20 μg) adsorbed to Alhydrogel®. The cavity-filling mutants were considerably more effective at eliciting TNA than RiVax (Fig. 2A, B). Although the differences in ricin-specific serum IgG levels among the groups were less pronounced after the second boost (Fig. S3B), three of the derivatives (RB, SA, and SB) still had significantly higher TNA levels than those observed in RiVax-immunized animals (Fig. 2B). In fact, TNA levels in sera of RB-immunized mice were 5–6 times greater than those of RiVax-immunized mice. As expected, the immunized groups of mice all survived 10 x LD50 ricin challenge (Fig. 2C, D).

We next repeated the mouse immunization studies using a 4-fold lower dose of antigen (i.e., 5 μg) to determine whether the differences in immunogenicity were more pronounced under conditions of limiting antigen. At the lower dose, we observed that RB was consistently superior to RiVax and the other RiVax derivatives at eliciting TNA (Fig. 2E, F). After the first boost, 6/8 of the RB-immunized mice had detectable TNA, whereas only 1/8 of the RiVax-immunized mice had detectable TNA. After the second boost, 8/8 mice immunized with RB had detectable serum TNA as compared to only 2/8 in the RiVax-immunized mice. These data demonstrate that RB elicits a more immunogenic ricin neutralizing antibody response *in vivo* than RiVax or the RiVax derivatives.

Immunogenicity of RC, a RiVax triple mutant with enhanced thermostablity

We previously postulated that there might be a relationship between the thermostability of RiVax and its immunogenicity as a vaccine antigen, such that more thermostable derivatives of RiVax would be more immunogenic and adept at eliciting TNA [31]. To test this possibility,

we produced a cavity-filling variant of RB with the express intent of increasing its overall thermal stability. Computational modeling suggested that the introduction of isoleucine (V81I) rather than leucine (V81L) at position 81 would increase local packing and thereby thermostability. We produced this mutant and refer to as simply RC (V81I/C171L/V204I). As such, RC differs from RB at only position 81.

The introduction of isoleucine at position 81, replacing valine (V81I), affected the thermostability of the protein by ~ 4 °C relative to RiVax or the other four cavity filling mutants (Table 2; Figure 3A). Relative to RiVax, RC gained ~4 °C of stability as measured by CD, greater than any of the other derivatives (Fig. 3A). RC gained ~2 °C in stability as measured by fluorescence melting point and also thermally shifted the static light scattering signal by 2 °C (Fig. 3B, C). RC was the only mutant showing a significant shift in thermal stability by DSC relative to RiVax in both transition regions, with a 3 to 4 °C difference in Tm (Fig. 3D).

To determine what effect the V81I mutation had on the immunogenicity of RiVax, groups of mice were immunized by the s.c. route with RiVax, RB, or RC, each adsorbed to Alhydrogel. Analysis of sera collected from mice 1 week or 10 weeks after the second booster immunization revealed RB or RC immunization resulted in TNA titers that were significantly higher (~10 fold) than those observed in RiVax-immunized animals (Figure 4). However, contrary to our hypothesis, RC was no more effective than RB at eliciting TNA, demonstrating that the slight enhancement in overall thermostability did not translate into a more immunogenic antigen (Figure 4). Nonetheless, these data constitute further evidence that RB (as well as RC) is a more immunogenic vaccine antigen than RiVax and underscores the need to determine the immunological basis for this increased activity.

Quantitative stability/flexibility relationships of RiVax mutants

To glean insight into the structural basis for the increased immunogenicity conferred by the RB and RC constructs, and increased stability in RC, a QSFR analysis was performed on RiVax (PDBID: 3SRP) and its mutants (RA, RB, RC, SA, SB) in the native and transition states. It was found that RiVax and all five mutants have virtually the same backbone flexibility in the native state, with only two notable differences. First, all mutants are slightly less flexible in the region at residues 20 to 28, and mutants RA, RB and RC became more flexible at residue 180. In the transition state, RB has the greatest backbone flexibility within the beta-sheet region at residues 55 to 95. RC is less flexible than RiVax in a few regions, most notably within the beta-hairpin turn at residues 225 to 245.

Greater differences occur in residue pair couplings quantified by the CC-plots. The CC-plot for mutant RB in the native state (Figure 5A) shows that RB is more rigidly correlated than RiVax in regions that span residues from the N-terminus to residue 45, residues 98–103, and from residue 200 to the C-terminus. As such, RB restricts the N- and C-termini motions compared to RiVax in the native state. Moreover, these two swaths of restricted motions couple to residues 98–103, which lie within one of the two B-cell epitopes at Asn97–Phe108 [40]. Despite this broad range of rigidification, two localized regions around residue 150 and 177 become more flexibly correlated to one another compared to RiVax. It is worth

noting that in all 5 mutants, the regions 18–32, 98–103 and 210–218 become more rigidly correlated.

In contrast, RB has much greater flexibly correlated motions relative to RiVax in the transition state within regions that span residues 7–30, 55–90 and 137–200 (Figure 5B), in addition to the two localized regions around residue 150 and 177. Because the difference CC-plot between RC and RB in the native state (Figure 5C) shows up as mostly white, this indicates that RB and RC share similar characteristics in the native state. However, the region that spans residues 7 through 17 and the region that spans residues 202 to 205 are more flexibly correlated and are coupled to one another. Within the region that spans residues 210 to 250, RC mechanically stabilizes the native state the most, although RB is a close second.

The difference CC-plot between RC with respect to RB in the transition state (Figure 5D) clearly shows that RC also mechanically stabilizes the transition state more than RB. Interestingly, RC is most similar to RB in the native state, and most similar to RA in the transition state (data not shown). The special property about RC is that it appears to be most effective in mechanically stabilizing both the native state and transition state among all five of the mutants analyzed.

An effective way to visualize the greatest changes in residue-pair correlations is to cluster the most significant changes in correlations within a difference CC-plot (i.e. elements with SBNR>1) and map these changes onto the protein structure (Figure 6). Juxtaposition is made between mutants RB and RC to visualize on the structure how they differ from RiVax in both the native and transition states. While RC is slightly more effective than RB in increasing mechanical stability relative to RiVax in the native state, the effectiveness of RC in increasing mechanical stability is much greater than RB in the transition state. Therefore, mutant RC is found to be the most effective alternative mutant for mechanically stabilizing both the native and transition state, while providing the greatest thermodynamic gain in stability together with a comparatively large kinetic free energy barrier.

Discussion

The poor immunogenicity of recombinant non-oligomeric protein antigens constitutes a significant impediment to the development of a number of subunit vaccines for biodefense, including ricin toxin [3]. In this study we employed a computational strategy as a means to produce derivatives of a leading ricin toxin subunit vaccine, RiVax, with an enhanced capacity to elicit toxin-neutralizing antibodies in mice following a prime-boost regimen. Of the five RiVax derivatives that we evaluated the most promising was RB, which carries the three point mutations, V81L, C171L and V204I, in addition to RiVax's original V76M and Y80A mutations. The improvement of RB over RiVax was most evident in the low dose immunization studies in which 6/8 of the RB-immunized mice had detectable TNA, whereas only 1/8 of the RiVax-immunized mice had detectable TNA. After the second boost, 8/8 mice immunized with RB had detectable serum TNA as compared to only 2/8 in the RiVax-immunized mice. The closely related RC mutant, which differs from RB only by the substitution of Ile at 81 that renders the protein slightly more thermostable was also

significantly more immunogenic than RiVax, although no better than RB when tested side-by-side in mice.

To understand why RB and RC were more immunogenic than RiVax, a comparative QSFR analysis was performed. We posit that the flexibility of domains might influence the immunogenicity of specific regions, permitting access to epitopes that are closer in structure to native RTA. Previously, immunodominant regions on RTA had been identified in the presence of mouse and rabbit sera [40]. The QSFR analysis showed that overall backbone flexibility was not altered significantly by any of the mutations, except that RA, RB and RC increased flexibility at residue 180. However, for residue-pair couplings, it was found that RB and RC mechanically stabilizes both the N- and C-termini regions through correlated rigidity in the native state more than all other mutants, and this rigidification extends to residues 98 to 103 that overlapped with immunodominant regions II and V. In addition, RB and RC increased correlated flexibility between residues 150 and 177 in the native state related to immunodominant regions III and IV respectively [40]. Even small differences in the flexibility or accessibility of these domains could have a profound effect on the “quality” of antibodies elicited upon immunization, considering that we estimated that roughly 90% of RTA-specific B cell epitopes are conformational (discontinuous) in nature [40,52]. Alternatively, the packing mutations could influence antigen stability in situ (e.g., limit protease sensitivity) or even following adsorption onto aluminum salts, thereby prolonging the duration of antibody release and/or deposition in tissue [53].

Further examination is required to detail the residues that were mutated in RB and RC and how they might affect overall immunogenicity and/or stability of RiVax. Residues 13–25, including V18 have been tentatively identified as being the target of several so-called Cluster 2 toxin-neutralizing monoclonal antibodies like SyH7 (R. Toth, D. Volkin, CR. Middaugh, N. Mantis, manuscript in preparation). Residue V81 is situated within β-strand F and next to a key residue associated with the active site, Y80. We have recently identified a monoclonal antibody that associates with T80 and possibly V81, thereby evoking a possible role of this residue in antibody recognition (D. Vance, M. Rudolph and N. Mantis, manuscript in preparation). Residue C171 is located within α-helix E, part of which is the target of several known neutralizing mAbs, including GD12. However, it should be noted that C171 is buried and therefore not surface accessible so it is unclear whether mutations at this site act locally or distally. Residue V204 is situated within α-helix G. There are no known B cell epitopes within this region, probably because the region is buried and not surface accessible. Finally, residue S228 is situated within the C-terminus of RTA that normally interfaces with RTB. This region is devoid of secondary structure, but it has been suggested that the C-terminus of RiVax (in the absence of RTB) is readily unfolded and promotes instability of the protein. It is possible that mutation S228 augments immunity by stabilizing the labile nature of the C-terminus. Regardless of the actual mechanism by which mutations within RB and RC potentiate the antibody response to ricin, further studies on these antigens are warranted in rabbits and non-human primates. These studies will determine whether the novel RiVax derivatives actually confer a benefit worth the resources required for advanced development.

Supplementary Material

Refer to Web version on PubMed Central for supplementary material.

Acknowledgments

The authors would like to thank Dr. Robert N. Brey (Soligenix) for helpful discussions and Dr. Fei P. Gao (KU) for his assistance with protein production.

This work was supported by NIH grants U01AI082210, 8P20GM103420, and 5P20RR017708 as well as a research grant from the Kauffman Foundation, Kansas City, MO. JCT acknowledges financial support from NIH T32 GM008359 and a pre-doctoral fellowship from the PhRMA Foundation, Washington, D.C. ES acknowledges financial support from NIH T32 AI055429 (PI: McDonough).

The following abbreviations are used

DSC	differential scanning calorimetry
T_m	melting temperature
RA	RiVax derivative V81I/V204I
RB	RiVax derivative V81L/C171L/V204I
RC	RiVax derivative V81I/C171L/V204I
RTA	ricin toxin A chain
RTB	ricin toxin B chain
SA	RiVax derivate V18P/C171V
SB	RiVax derivative C171V/S228K
TNA	toxin neutralizing antibody
TEV	tobacco etch virus
MOE	Molecular Operating Environment
SBNR	signal beyond noise ratio
QSFR	quantitative stability/flexibility relationships
NSE	native state ensembles
TSE	transition state ensembles
mDCM	minimum distance constraint model

References

1. Alving CR, Peachman KK, Rao M, Reed SG. Adjuvants for human vaccines. Curr Opin Immunol. 2012; 24(3):310–315. [PubMed: 22521140]
2. Dormitzer PR, Grandi G, Rappuoli R. Structural vaccinology starts to deliver. Nat Rev Microbiol. 2012; 10(12):807–813. [PubMed: 23154260]
3. Wolfe DN, Florence W, Bryant P. Current biodefense vaccine programs and challenges. Hum Vaccin Immunother. 2013; 9(7)
4. Stirpe F, Battelli MG. Ribosome-inactivating proteins: progress and problems. Cell Mol Life Sci. 2006; 63(16):1850–1866. [PubMed: 16799768]

5. O'Hara JM, Yermakova A, Mantis NJ. Immunity to ricin: fundamental insights into toxin-antibody interactions. Curr Top Microbiol Immunol. 2012; 357:209–241. [PubMed: 22113742]
6. Sandvig K, Torgersen ML, Engedal N, Skotland T, Iversen TG. Protein toxins from plants and bacteria: probes for intracellular transport and tools in medicine. FEBS Lett. 2010; 584(12):2626–2634. [PubMed: 20385131]
7. Rutenber E, Ready M, Robertus JD. Structure and evolution of ricin B chain. Nature. 1987; 326(6113):624–626. [PubMed: 3561502]
8. Sandvig K, Olsnes S, Pihl A. Kinetics of binding of the toxic lectins abrin and ricin to surface receptors of human cells. J Biol Chem. 1976; 251(13):3977–3984. [PubMed: 6468]
9. Spooner RA, Lord JM. How Ricin and Shiga Toxin Reach the Cytosol of Target Cells: Retrotranslocation from the Endoplasmic Reticulum. Curr Top Microbiol Immunol. 2012; 357:19–40. [PubMed: 21761287]
10. Endo Y, Tsurugi K. RNA N-glycosidase activity of ricin A-chain. Mechanism of action of the toxic lectin ricin on eukaryotic ribosomes. J Biol Chem. 1987; 262(17):8128–8130. [PubMed: 3036799]
11. Jandhyala DM, Thorpe CM, Magun B. Ricin and Shiga toxins: effects on host cell signal transduction. Curr Top Microbiol Immunol. 2012; 357:41–65. [PubMed: 22057792]
12. Radosavljevic V, Belojevic G. A new model of bioterrorism risk assessment. Biosecur Bioterror. 2009; 7(4):443–451. [PubMed: 20028253]
13. Griffiths GD. Understanding ricin from a defensive viewpoint. Toxins (Basel). 2011; 3(11):1373–1392. [PubMed: 22174975]
14. Reisler RB, Smith LA. The need for continued development of ricin countermeasures. Adv Prev Med. 2012; 2012:149737. [PubMed: 22536516]
15. O'Hara JM, Brey RN, Mantis NJ. Comparative Efficacy in Mice of Two Lead Candidate Ricin Toxin A Subunit (RTA) Vaccine. Clinical and Vaccine Immunology. 2013 in press.
16. Smallshaw JE, Vitetta ES. Ricin Vaccine Development. Curr Top Microbiol Immunol. 2012; 357:259–272. [PubMed: 21805396]
17. Smallshaw JE, Firan A, Fulmer JR, Ruback SL, Ghetie V, Vitetta ES. A novel recombinant vaccine which protects mice against ricin intoxication. Vaccine. 2002; 20(27–28):3422–3427. [PubMed: 12213413]
18. Smallshaw JE, Ghetie V, Rizo J, Fulmer JR, Trahan LL, Ghetie MA, Vitetta ES. Genetic engineering of an immunotoxin to eliminate pulmonary vascular leak in mice. Nat Biotechnol. 2003; 21(4):387–391. [PubMed: 12627168]
19. Legler PM, Brey RN, Smallshaw JE, Vitetta ES, Millard CB. Structure of RiVax: a recombinant ricin vaccine. Acta Crystallogr D Biol Crystallogr. 2011; 67(Pt 9):826–830. [PubMed: 21904036]
20. Greene CJ, Chadwick CM, Mandell LM, Hu JC, O'Hara JM, Brey RN 3rd, Mantis NJ, Connell TD. LT-IIb(T13I), a non-toxic type II heat-labile enterotoxin, augments the capacity of a ricin toxin subunit vaccine to evoke neutralizing antibodies and protective immunity. PloS one. 2013; 8(8):e69678. [PubMed: 23936344]
21. Marconescu PS, Smallshaw JE, Pop LM, Ruback SL, Vitetta ES. Intradermal administration of RiVax protects mice from mucosal and systemic ricin intoxication. Vaccine. 2010; 28(32):5315–5322. [PubMed: 20562013]
22. Neal LM, McCarthy EA, Morris CR, Mantis NJ. Vaccine-induced intestinal immunity to ricin toxin in the absence of secretory IgA. Vaccine. 2011; 29(4):681–689. [PubMed: 21115050]
23. Smallshaw JE, Richardson JA, Vitetta ES. RiVax, a recombinant ricin subunit vaccine, protects mice against ricin delivered by gavage or aerosol. Vaccine. 2007; 25(42):7459–7469. [PubMed: 17875350]
24. Vitetta ES, Smallshaw JE, Coleman E, Jafri H, Foster C, Munford R, Schindler J. A pilot clinical trial of a recombinant ricin vaccine in normal humans. Proceedings of the National Academy of Sciences of the United States of America. 2006; 103(7):2268–2273. [PubMed: 16461456]
25. Vitetta ES, Smallshaw JE, Schindler J. Pilot phase IB clinical trial of an alhydrogel-adsorbed recombinant ricin vaccine. Clinical and Vaccine Immunology. 2012; 19(10):1697–1699. [PubMed: 22914366]

26. Vance DJ, Rong Y, Brey RN, Mantis NJ. Combination of two candidate subunit vaccine antigens elicits protective immunity to ricin and anthrax toxin in mice. Vaccine. 2015; 33(3):417–421. [PubMed: 25475957]
27. Argent RH, Parrott AM, Day PJ, Roberts LM, Stockley PG, Lord JM, Radford SE. Ribosome-mediated folding of partially unfolded ricin A-chain. J Biol Chem. 2000; 275(13):9263–9269. [PubMed: 10734065]
28. Compton JR, Legler PM, Clingan BV, Olson MA, Millard CB. Introduction of a disulfide bond leads to stabilization and crystallization of a ricin immunogen. Proteins. 2011; 79(4):1048–1060. [PubMed: 21387408]
29. McHugh CA, Tammariello RF, Millard CB, Carra JH. Improved stability of a protein vaccine through elimination of a partially unfolded state. Protein Sci. 2004; 13(10):2736–2743. [PubMed: 15340172]
30. Olson MA, Carra JH, Roxas-Duncan V, Wannemacher RW, Smith LA, Millard CB. Finding a new vaccine in the ricin protein fold. Protein Eng Des Sel. 2004; 17(4):391–397. [PubMed: 15187223]
31. Thomas JC, O'Hara JM, Hu L, Gao FP, Joshi SB, Volkin DB, Brey RN, Fang J, Karanicolas J, Mantis NJ, Middaugh CR. Effect of single-point mutations on the stability and immunogenicity of a recombinant ricin A chain subunit vaccine antigen. Hum Vaccin Immunother. 2013; 9(4):740–748.
32. Das R, Baker D. Macromolecular modeling with rosetta. Annu Rev Biochem. 2008; 77:363–382. [PubMed: 18410248]
33. Leaver-Fay A, Tyka M, Lewis SM, Lange OF, Thompson J, Jacak R, Kaufman K, Renfrew PD, Smith CA, Sheffler W. ROSETTA3: an object-oriented software suite for the simulation and design of macromolecules. Methods in enzymology. 2011; 487:545. [PubMed: 21187238]
34. Friedland GD, Linares AJ, Smith CA, Kortemme T. A simple model of backbone flexibility improves modeling of side-chain conformational variability. J Mol Biol. 2008; 380(4):757–774. [PubMed: 18547586]
35. Smith CA, Kortemme T. Backrub-like backbone simulation recapitulates natural protein conformational variability and improves mutant side-chain prediction. J Mol Biol. 2008; 380(4): 742–756. [PubMed: 18547585]
36. Sheffler W, Baker D. RosettaHoles: rapid assessment of protein core packing for structure prediction, refinement, design, and validation. Protein Science. 2009; 18(1):229–239. [PubMed: 19177366]
37. Li Y, Middaugh CR, Fang J. A novel scoring function for discriminating hyperthermophilic and mesophilic proteins with application to predicting relative thermostability of protein mutants. BMC bioinformatics. 2010; 11(1):62. [PubMed: 20109199]
38. Li Y, Zhang J, Tai D, Russell Middaugh C, Zhang Y, Fang J. Prots: A fragment based protein thermo-stability potential. Proteins: Structure, Function, and Bioinformatics. 2012; 80(1):81–92.
39. Cordes MH, Sauer RT. Tolerance of a protein to multiple polar-to-hydrophobic surface substitutions. Protein science. 1999; 8(02):318–325. [PubMed: 10048325]
40. O'Hara JM, Neal LM, McCarthy EA, Kasten-Jolly JA, Brey RN 3rd, Mantis NJ. Folding domains within the ricin toxin A subunit as targets of protective antibodies. Vaccine. 2010; 28:7035–7046. [PubMed: 20727394]
41. Jacobs DJ, Dallakyan S, Wood G, Heckathorne A. Network rigidity at finite temperature: relationships between thermodynamic stability, the nonadditivity of entropy, and cooperativity in molecular systems. Physical Review E. 2003; 68(6):061109.
42. Jacobs DJ, Dallakyan S. Elucidating protein thermodynamics from the three-dimensional structure of the native state using network rigidity. Biophysical journal. 2005; 88(2):903–915. [PubMed: 15542549]
43. Vorov OK, Livesay DR, Jacobs DJ. Nonadditivity in conformational entropy upon molecular rigidification reveals a universal mechanism affecting folding cooperativity. Biophysical journal. 2011; 100(4):1129–1138. [PubMed: 21320459]
44. Jacobs DJ. Ensemble-based methods for describing protein dynamics. Current opinion in pharmacology. 2010; 10(6):760–769. [PubMed: 20965786]

45. Jacobs, DJ. An Interfacial Thermodynamics Model for Protein Stability. In: Misra, AN., editor. Biophysics. InTech; 2012. p. 91-132.

46. Jacobs D, Rader A, Kuhn L, Thorpe M. Graph theory predictions of protein flexibility. Proteins: Struct Funct Genet. 2001; 44:150–155. [PubMed: 11391777]

47. Livesay D, Dallakyan S, Wood G, Jacobs D. A flexible approach for understanding protein stability. FEBS letters. 2004; 576(3):468–476. [PubMed: 15498582]

48. Livesay DR, Jacobs DJ. Conserved quantitative stability/flexibility relationships (QSFR) in an orthologous RNase H pair. PROTEINS: Structure, Function, and Bioinformatics. 2006; 62(1):130–143.

49. Jacobs DJ, Livesay DR, Hules J, Tasayco ML. Elucidating quantitative stability/flexibility relationships within thioredoxin and its fragments using a distance constraint model. Journal of molecular biology. 2006; 358(3):882–904. [PubMed: 16542678]

50. Li T, Verma D, Tracka M, Casas-Finet J, Livesay D, Jacobs D. Thermodynamic Stability and Flexibility Characteristics of Antibody Fragment Complexes. Protein and peptide letters. 2013; 21(8):752–765. [PubMed: 23855672]

51. Carra JH, McHugh CA, Mulligan S, Machiesky LM, Soares AS, Millard CB. Fragment-based identification of determinants of conformational and spectroscopic change at the ricin active site. BMC structural biology. 2007; 7(1):72. [PubMed: 17986339]

52. O'Hara JM, Kasten-Jolly JC, Reynolds CE, Mantis NJ. Localization of non-linear neutralizing B cell epitopes on ricin toxin's enzymatic subunit (RTA). Immunology letters. 2014; 158(1–2):7–13. [PubMed: 24269767]

53. Hem SL, Hogenesch H. Relationship between physical and chemical properties of aluminum-containing adjuvants and immunopotentiation. Expert review of vaccines. 2007; 6(5):685–698. [PubMed: 17931150]

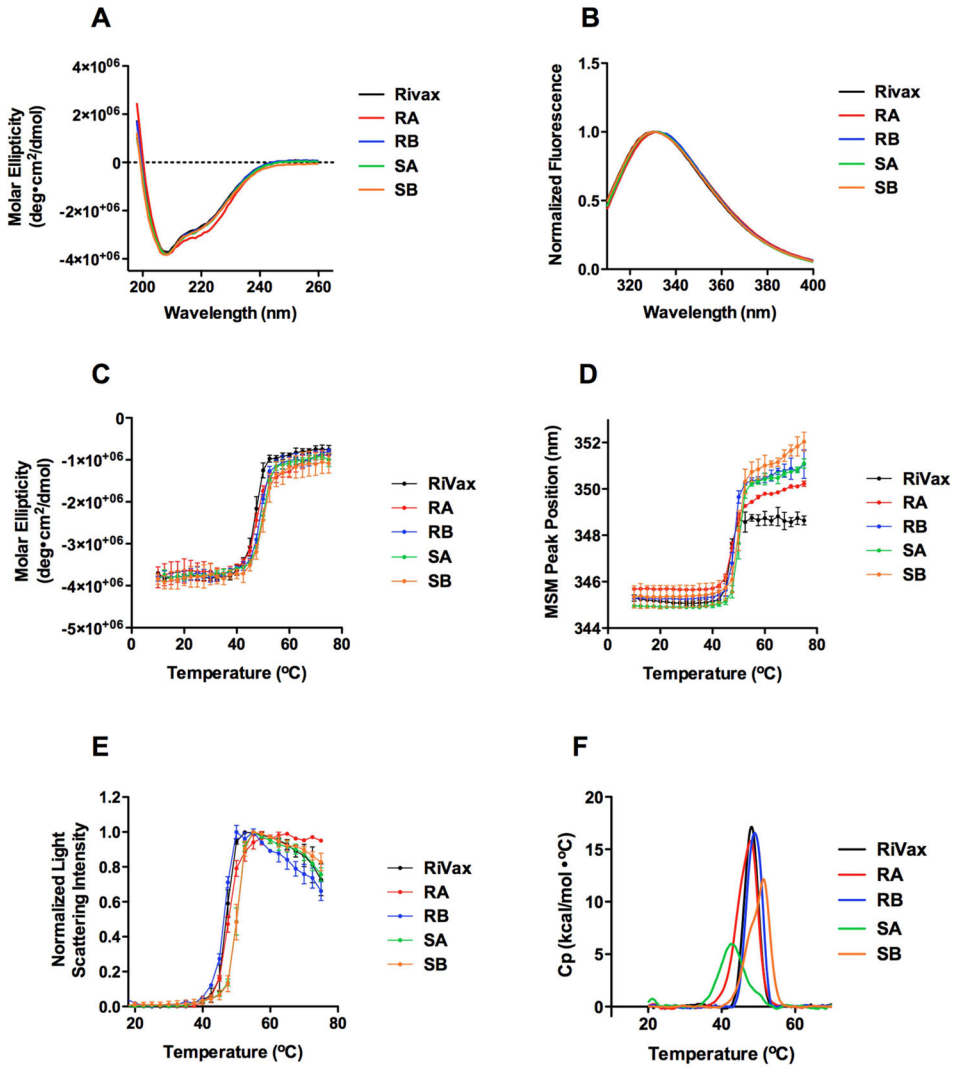

Figure 1. Structural integrity and conformation stability of RiVax and RiVax derivatives, RA, RB, SA, and SB

CD confirms the secondary structure content of variants RB, SA, and SB are identical to that of RiVax, while RA is slightly perturbed (A). Fluorescence emission spectroscopy reveals that the active site environment of variants RB, SA, and SB are indistinguishable from that of RiVax, while RA displays a slightly perturbed structure in which the tryptophan residue near the active site is exposed to a mildly more polar environment (B). Molar ellipticity at 208 nm vs. temperature, monitors the stability of helical regions (C). Tryptophan fluorescence monitors the change in tertiary structure vs. temperature near the active site (D). Light scattering at 295 nm monitors aggregation propensity (E). DSC detects two thermal transitions in which the low temperature transition is not detected by CD, fluorescence, or light scattering (F). The mutations exert most of their stabilizing effect on this transition, which we attribute to the C-terminal region of the proteins. Where applicable, error bars represent standard deviation (n = 3). Tm values are listed in Table 2.

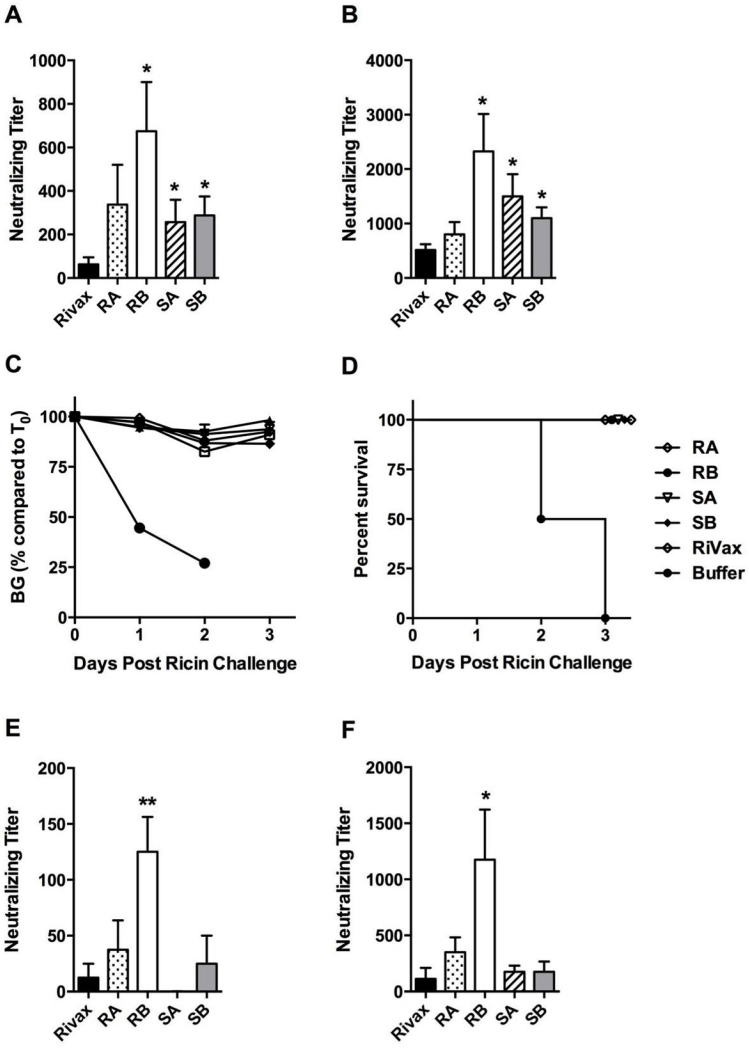

Figure 2. Toxin-neutralizing titers in sera of mice immunized with RiVax and RiVax derivatives. (Panels A–D)

Groups of mice (n = 8 mice/group) were immunized with 20 μg of RiVax or the indicated RiVax derivatives, each adsorbed to Alhydrogel. Serum samples were collected from the mice following the second (A) and third (B) immunizations and assessed for toxin-neutralzing activity in a Vero cell assay. Groups of animals were then challenged with 10xLD_{50} ricin, as described in the Materials and Methods. (C) Hypoglycermia was used as a measure of ricin intoxication. (D) Survival curves following ricin challenge. **(Panels E and F)** Groups of mice (n = 8 mice/group) were immunized with 5 μg of RiVax or the indicated RiVax derivatives adsorbed to Alhydrogel, as in Panels A-D. Serum samples were collected from the mice following the second (E) and third (F) immunizations and assessed for toxin-neutralizing activity. An unpaired t-test comparing each variant to RiVax was used to compute statistical significance.* $p < 0.05$, ** $p < 0.01$.

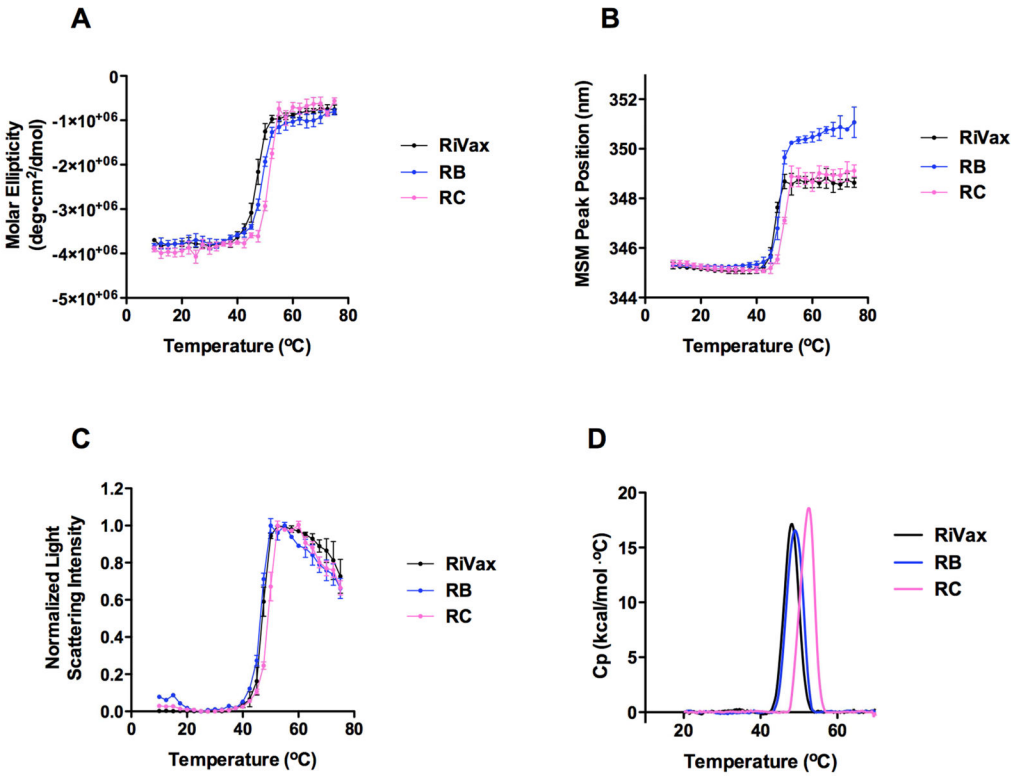

Figure 3. Thermal stability of RiVax and RiVax derivatives, RB and RC

Molar ellipticity at 208 nm monitors the thermal stability of helical regions (A). Tryptophan fluorescence monitors thermal stability of the tertiary structure near the active site (B). Light scattering at 295 nm monitors aggregation propensity (C). DSC detects two thermal transitions in which the low temperature transition is not detected by CD, fluorescence, or light scattering (D). Where applicable, error bars represent standard deviation (n = 3). Tm values are listed in Table 2.

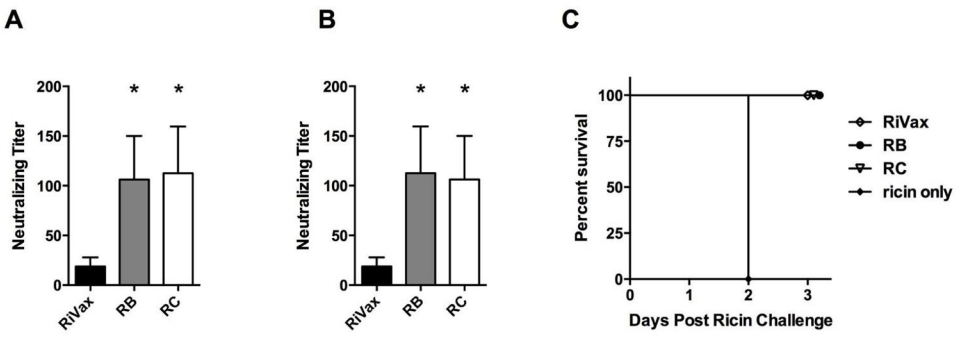

Figure 4. Toxin-neutralizing titers in sera of mice immunized with RB and RC derivatives

Groups of mice (n = 8 mice/group) were immunized with 5μg of RiVax, RB or RC adsorbed to Alhydrogel. Serum samples were collected from the mice following the second (A) and third (B) immunizations and assessed for toxin-neutralzing activity in a Vero cell assay. (C) Groups of animals were then challenged with 10xLD_{50} ricin, as described in the Materials and Methods. An unpaired t-test comparing each variant to RiVax was used to compute statistical significance.* $p < 0.05$, ** $p < 0.01$.

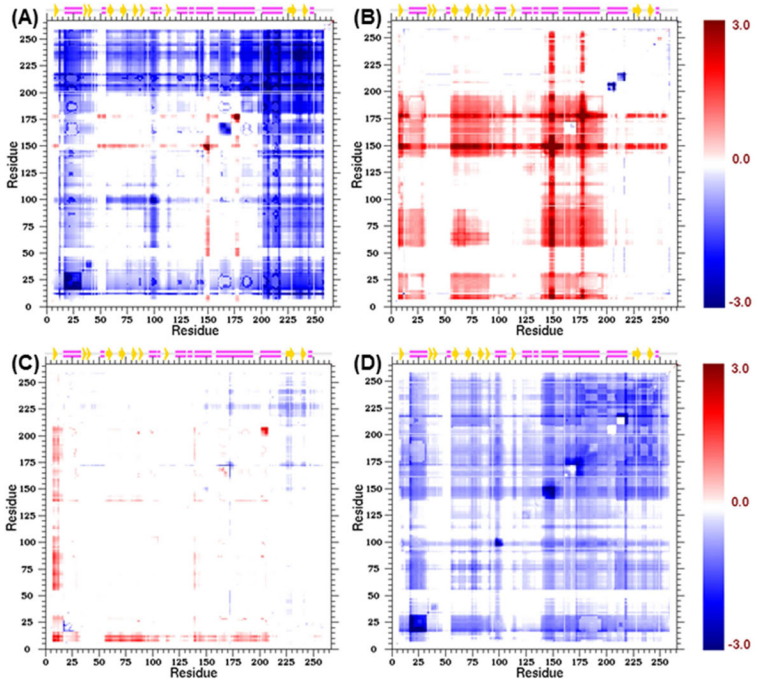

Figure 5. Cooperativity Correlation Difference Plots

Correlation in flexibility and rigidity between residue pairs is described by CC-plots. Differences in CC-plots are shown for mutant RB relative to RiVax in the native state (A) and the transition state (B). Difference CC-plots are shown for mutant RC relative to mutant RB in the native state (C) and the transition state (D). The coloring scale is the same for all panels, representing the *signal beyond noise ratio* (SBNR) as defined in the text. White regions correspond to places that are un-correlated or are filtered out because of weak correlations with magnitude less than baseline noise. Red and blue regions correspond to correlated flexibility and correlated rigidity respectively. Note that the number 3 on the color scale corresponds to a signal strength that is 3 standard deviations beyond noise.

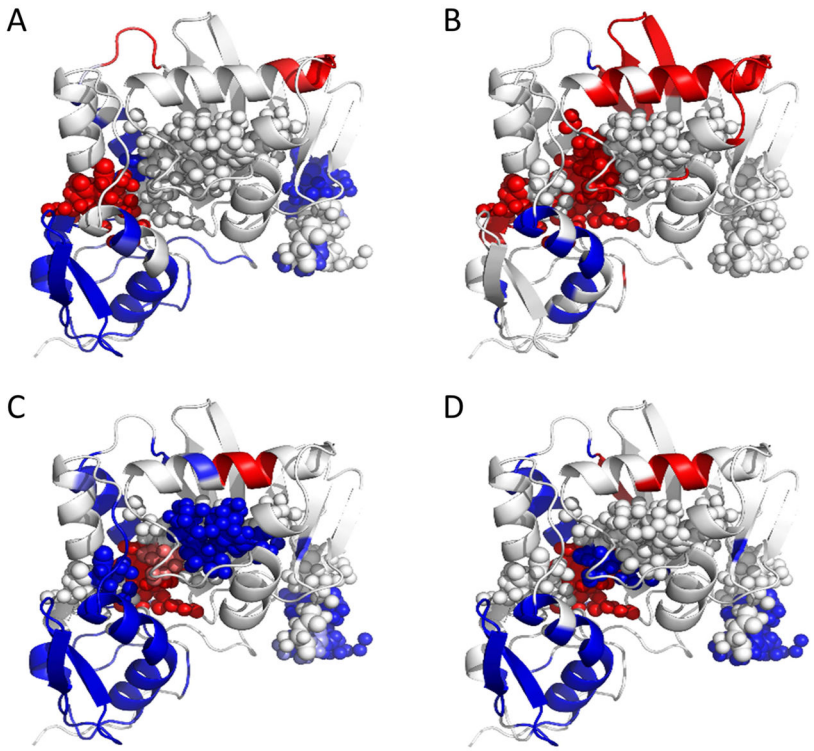

Figure 6. Extreme Backbone Cooperativity Correlation

The most significant correlations obtained from difference CC-plots are rendered onto protein models (mutated from PDB: 3SRP) for RB relative to RiVax in the native state (A) and the transition state (B), and for RC relative to RiVax in the native state (C) and the transition state (D). The color scale represents the signal beyond noise ratio (SBNR), and inherits the same color scale employed in the difference plots. The small spheres show backbone atoms that fall in immunologically important regions.

Table 1

RiVax derivatives used in this study

Antigen	Mutations	Design Basis
RiVax	Y80A/V76M	N/A[a]
RA	V81I/V204I	Rosetta[b]
RB	V81L/C171L/V204I	Rosetta
RC	V81I/C171L/V204I	Rosetta
SA	V18P/C171V	Scoring function[c]
SB	C171V/S228K	Scoring function

[a]Parent vaccine antigen to which mutations were introduced;

[b]Mutations were designed to fill packing defects in RiVax by increasing the volume of sidechains adjacent to cavities;

[c]Mutations were designed on the basis of a scoring function that predicts the relative stability of proteins and their mutants.

Table 2

Transition melting temperatures (T_m(°C)) and changes in enthalpy of RiVax and RiVax derivatives[a,b]

Antigen	CD	Fluorescence	Light scattering	DSC			
				$T_{m,1}$app	ΔH_1 app (kcal/mol)	$T_{m,2}$ app	ΔH_2 app (kcal/mol)
RiVax	47.8 ± 0.5	47.8 ± 0.1	47.1 ± 0.1	47.9 ± 0.2	2.0 ± 0.3	48.8 ± 0.6	2.4 ± 0.2
RA	47.9 ± 0.1	48.0 ± 0.2	47.5 ± 0.3	45.8 ± 0.1	4.0 ± 0.1	48.5 ± 0.0	0.3 ± 0.0
RB	48.8 ± 0.3	48.8 ± 0.5	47.1 ± 0.3	47.5 ± 0.2	2.9 ± 0.1	49.6 ± 0.4	3.0 ± 0.1
RC	52.2 ± 0.4	50.2 ± 0.3	49.8 ± 0.1	51.7 ± 0.2	2.4 ± 0.1	52.1 ± 0.3	2.8 ± 0.1
SA	49.6 ± 0.4	49.9 ± 0.3	50.1 ± 0.2	42.8 ± 0.1	5.0 ± 0.2	50.0 ± 0.1	2.7 ± 0.1
SB	49.9 ± 0.3	49.8 ± 0.5	49.9 ± 0.5	48.2 ± 0.0	4.4 ± 0.5	51.7 ± 0.0	3.9 ± 0.3

[a] $T_{m\ app}$ and H_{app} values in 20 mM citrate phosphate buffer (pH 7), 0.15 ionic strength by addition of sodium chloride

[b] $T_{m\ app}$ and H_{app} values are termed apparent due to irreversible thermal transitions.